TITLE: AN ELECTROSTRATIGRAPHIC CROSS-SECTION ACROSS THE CENTRAL PO PLAIN: BEARINGS ON SUBSURFACE GEOLOGY AND HYDROSTRATIGRAPHY.

Mele M.[1,3], Bersezio R.[1], Giudici M.[2]

[1] Dipartimento di Scienze della Terra "A. Desio", Università degli Studi di Milano, via Mangiagalli 34, 20133 Milano, Italy

[2] Dipartimento di Scienze della Terra "A. Desio", Università degli Studi di Milano, via Cicognara 7, 20129 Milano, Italy

[3] Geo360 Studio, Via Cimbardi 55, 20062 Cassano d'Adda, Italy

Corresponding author: Mauro Mele

e-mail: mauro.mele@unimi.it

ABSTRACT

A 72-kilometers-long N-S cross-section was surveyed with Direct Current resistivity soundings through the Quaternary clastic infill of the Apennine foredeep in the Po plain of Lombardy (Northern Italy). The aims are: 1) to test the potential of DC resistivity methods at the regional scale; 2) to draw the electrostratigraphic picture of the basin fill, down to the pre-Quaternary substratum; 3) to refine and test the methodology and concepts of hierarchic electrostratigraphy at the basin scale; 4) to contribute to characterize the regional hydrostratigraphy of a relevant hydrogeological basin. 163 resistivity-versus-depth profiles with a maximum investigation depth of 450 m were obtained from Vertical Electrical Soundings. To draw the electrostratigraphic cross-section, the polarity of the resistivity contrast across resistivity interfaces (i.e., resistive over conductive layers or vice-versa) was considered and the discontinuities were correlated according to the persisting pattern form North to South. Doing so, the hierarchic assemblage of four major electrostratigraphic boundaries and the five intervening Groups of Electrostratigraphic Units (EsUs) was established. The resulting picture was compared to the available subsurface reconstructions from

literature, using the 1-D borehole data only to check the geophysical image at some random sample sites. The results show that the electrostratigraphic picture captures the geological and hydrostratigraphic complexity of the subsurface of the basin comparing well with the available direct subsurface geological and hydrostratigraphic reconstructions. At the regional scale of the cross-section, two hierarchic orders of EsUs and correlative boundaries could be drawn (1st order Groups and 2nd order individual EsUs), while the lowermost 3rd order rank, the electrolayer, is recognised at the single VES sites only.

Key-words: Electrostratigraphy, Hydrogeophysics, Hydrostratigraphy, Po Plain, Quaternary, Resistivity, VES.

1. INTRODUCTION

The subsurface of densely-populated alluvial plains of the world is the subject of geological, hydrogeological and geophysical studies, at both regional and local scales. Targets are both "deep" (for instance oil and gas reservoirs or high-temperature geothermal fields, hundreds to thousands of meters below the ground surface) and "shallow" (for instance groundwater reservoirs, low-temperature geothermal resources and so on, tens to hundreds of meters deep) and are related to a large number of diverse applications.

The shape of the basin-wide sedimentary units, their internal heterogeneities and the hierarchic arrangement of marine to continental clastic regressive sequences, that typically represent the shallow subsurface setting in alluvial basins, are the key-elements for a comprehensive characterization of these areas. Such a characterization can be approached by the integration of stratigraphic analysis and geophysical methods (Binley et al. 2010; Bridge and Hyndman 2004; Rubin and Hubbard 2005; Giudici 2010; Giudici et al. 2015).

To this purpose, ground-based Direct Current (DC) resistivity methods represent a cost-efficient tool to assist the hydrostratigraphical modelling of the alluvial stratigraphy. Thanks to the dependence of electrical properties on porosity, water saturation, pore water salinity, clay and silt content, grain size distribution, petrography and mineralogy of sediments (Keller and Frischknecht 1966; Reynolds 2011; Schön 2004; Slater 2007; Telford et al. 1990; Mele et al. 2014), DC methods allow the vertical survey of the subsoil by measuring the distortion of an electrical field applied at the ground surface by the variation of true electrical resistivity at depth.

Despite strong research and technological efforts, the reduction of the uncertainty on the geological interpretation of the subsurface resistivity images is still an open scientific problem. It greatly relies on the variation of the resolving

power of ground-based methods with the depth of investigation (Keller and Frischknecht 1966; Koefoed 1979) and, mostly, on the difficulty to match the electrical resistivity distribution in the subsurface with the geological data-set, such as fine-scale borehole-log stratigraphy.

Aiming to tackle these problems, in recent years an electrostratigraphic approach was set-up to manage resistivity data-sets in order to characterize geometries and internal properties of clastic, heterogeneous alluvial sequences (Bridge and Hyndman 2004; Huggenberger and Aigner 1999; Galloway and Sharp 1998). Mele et al. (2012) implemented the electrostratigraphic approach, describing the subsurface by DC methods in terms of 3-D volumes of sediments that, relatively with one another, maintain the same electrical resistivity contrast traceable in the subsurface wherever it exists. The resistivity contrast, in analogy to acoustic impedence for exploration seismic, is produced by the prominent geological and geometrical controlling factors on subsurface electrical conduction within the sedimentary sequence, i.e. gradual to sharp changes of clay/sand ratio, porosity, mineralogy of sediments, water content, water chemistry (mostly salinity) and temperature. These primary factors change through the subsurface in relation with the changes of thickness, shape, bedding styles and stacking patterns of the sedimentary bodies, including their pinch-outs, erosional truncations, folding and tectonic dips. Hence, the distribution of resistivity in the subsurface is expected to provide a proxy of the most relevant geological features at both the local and regional scales.

After a set of studies dedicated to improve and test the detailed resistivity imaging of the Po basin subsurface at the local scale (Bersezio et al. 2007; Mele et al. 2012, 2013, 2015), we now apply this approach to a wide scale case-study, that is the electrostratigraphy of a regional N-S cross-section across the Quaternary Po foreland basin in Northern Italy, East and South of Milan. The tectono-sedimentary setting of the basin is recorded by alluvial and glacio-fluvial clastic, regressive depositional systems, which prograde above shallow marine sediments, under the control of Pleistocene glacial cycles and Apennine-related tectonics. The resulting stacking patterns and the hydrogeochemistry of groundwater originate the geophysical contrasts between resistive (generally sands and gravels, i.e. coarse-grained “C”) and conductive intervals (clays and muds, i.e. fine-grained “F”, and the highly conductive connate waters). The magnitudes of these contrasts are suitable to be explored with ground-based DC methods.

Within a N-S strip across the central Po basin (Fig. 1) we formerly studied three fine-scale, key-sectors where we extensively acquired resistivity data with Vertical Electrical Soundings (VES; Mele et al. 2102, 2013, 2015). Our approach portrayed subsurface volumes of sediments that we informally named “Electrostratigraphic Units” (EsUs).

EsUs are characterised by specific, relatively small ranges of electrical resistivity and they are bounded by vertically- and laterally-persistent resistivity interfaces. In order to explain the results discussed in the paper, we introduce here the term "polarity" across a single resistivity interface (detectable by VES interpretation, see section 3.3) as the relative ordering of the resistivity overlap along the direction of increasing depth from earth surface, i.e. conductive-over-resistive (C-R pattern) or vice-versa (R-C pattern). In this way, EsUs are peculiar because they are defined on the basis of their resistivity, but the presence and nature of adjacent and overlapping units give rise to detectable electrical contrasts, traceable wherever their polarity is preserved, and permit the recognition of EsUs.

In particular, the results obtained at the key-sectors showed, as a whole, that a hierarchical structure of the EsUs emerges when exploring a sedimentary sequence; this structure is independent of any calibration between each VES and the lito-stratigraphy of a neighbouring 1-D borehole (Mele et al. 2012, 2013, 2015).

Owing to the expected decay of the VES vertical resolution with depth, the resistivity interfaces that bound the EsUs in the near-surface can be interpreted as individual and physically defined interfaces separating homogeneous sediments at the fine scale. On the contrary, at increasing depth, EsUs boundaries might be interpreted as *proxies* of the transition between sedimentary volumes with different styles of layering between conductive (clay-rich, i.e. fine-grained) versus resistive levels (sand-gravel rich, clay poor, i.e. coarse-grained), accounting for the variations of sediments' fluid saturation and chemistry (Mele et al. 2015). Hence, electrical resistivity within the EsUs can be interpreted as a *proxy* of a volume-averaged ratio between the "shale"-dominated conduction volumes and the "electrolytic"-dominated conduction volumes of the corresponding stratigraphic units. This ratio is similar to the net-to-gross ratio adopted in petroleum geology to represent the quality of a reservoir zone (Pirson 1958) and it is linked, through empirical petrophysical relationships, to bulk resistivity and to average pore-water conductivity (Mele et al. 2012).

Starting from these site-specific results, we now extend the application of the electrostratigraphic approach up to the regional scale across the Po basin (Fig. 1) with the following aims:

- to obtain a regional electrostratigraphic cross-section of a wide part of the Quaternary Po basin, South and East of Milan, orthogonal to the regional structural grain of the basin (Fig. 1);
- to complement the picture of the Plio-Quaternary sequences and structures of the Po foreland basin in Lombardy which are shown at shallow depth with low-resolution and some uncertainties by the currently available deep seismic images (Bresciani and Perotti 2014; Burrato et al. 2003; Cassano et al. 1986; Fantoni et al. 2004; Francese

et al. 2005; Ghielmi et al. 2013; Livio et al. 2009; Pieri and Groppi 1981; Toscani et al. 2014; Turrini et al. 2014), providing new insights on the debated Plio-Quaternary tectono-sedimentary evolution of the Po foreland basin;

- to generate electrostratigraphic images that can be interpreted in terms of hydrostratigraphy for the most relevant hydrogeological studies, showing the potential of the method in this field.

To all these purposes, here we describe and discuss a 72-kilometer-long regional resistivity cross-section, down to a maximum depth of 400 m below the ground surface (bgs from now on), in the central part of the Quaternary Po basin (Fig. 1). In this area, the cross-section crosses the Apennine foreland and extends from the buried front of the Northern Apennines, to the South, to the opposite flexured margin of Southern Alps to the North.

2. GEOLOGICAL SETTING OF THE CENTRAL PO PLAIN IN LOMBARDY

The Po plain represents the Neogene-Quaternary foreland basin shared by two opposite fold and thrust belts: from South to North, the Northern Apennines (verging North) and the Southern Alps (verging South; Fig. 1). In the subsurface of Lombardy, the buried frontal thrusts of the Apennine "Emilian Arc" interfere with the outermost Southalpine thrusts along an E-W belt, the Corneliano-Bordolano-Soresina interference zone (Bigi et al. 1990; Bersezio et al. 2001; Fantoni et al. 2004, Pieri and Groppi 1981). A gently South-dipping homocline of transgressive marine Pliocene sediments ("Pedealpine homocline", Pieri and Groppi 1981; Fig. 1) developed on the northern side of the basin, in unconformity above the Southalpine structures. The S–N sequence of fault-propagation folds, shaped the buried morphology with uplifted dome culminations alternating with synformal depocentres, the most prominent of which is the "Lodi synformal depocentre" (Fig. 1), and originated a set of isolated relieves which elevate above the terraced plain of Lombardy, on both the Apennines and Southern Alps sides. Some of these relieves (Fig.1) are either directly crossed by the electrostratigraphic cross-section (Casalpusterlengo – Codogno high)) or emerge in the neighbourhoods (San Colombano al Lambro and Zorlesco highs); or at some distance, like the Romanengo, M. Netto/Capriano del Colle and Castenedolo highs (Alfano and Mancuso 1996; Anfossi et al. 1971; Baio et al. 2004; Bersezio et al. 2010, 2016; Boni, 1967; Bresciani and Perotti, 2014; Burrato et al. 2003; Castiglioni and Pellegrini 2001; Cremaschi, 1987; Desio 1965; Livio et al., 2009; 2014; Pellegrini et al. 2003).

Deep seismic profiles showed the Messinian unconformity which truncates and seals the thrust-folded, syntectonic Tertiary clastic wedges and the overlaying marine Pliocene transgressive-regressive cycles (Cassano et al. 1986; Fantoni et al. 2001, Fantoni & Franciosi, 2010; Ghielmi et al. 2010, 2013; Pieri and Groppi, 1981; Rossi et al. 2015).

136 The Neogene succession is truncated after Apennine faulting and uplift as it is observed in outcrops (San Colombano
137 hill; Zuffetti et al. 2018) and in the subsurface (Codogno, Casalpusterlengo, Zorlesco and Chiesiolo buried structures;
138 Anfossi et al. 1971; Baio et al. 2004; Bersezio et al. 2010).

139 Four major seismic units, bounded by three regional unconformities, represent in the subsurface the transgressive-
140 regressive cycles of the latest Pliocene and Pleistocene that progressively led to the basin fill, under the concurrent
141 control of ongoing tectonics and glacio-isostatic evolution (Carminati et al. 2003; ENI- Regione Lombardia 2002;
142 Muttoni et al. 2003; Ori 1993). Deep seismic interpretation by Ghielmi et al. (2010, 2013) shows two major
143 unconformities, bounding three seismo-stratigraphic units, induced by the Early Pliocene (Zanclean) and Early
144 Pleistocene (Gelasian) Apennine increments of Northwards thrusting. Early Pleistocene deep-water clastics
145 unconformably overlay these former units (Ghielmi et al. 2010) and are covered by prograding fan deltas, coastal,
146 deltaic and fluvial sediments (Ori 1993) both on the alpine and Apennine sides of the Po basin. The middle
147 Pleistocene periglacial to glacio-fluvial successions spread all over the Lombardy Po plain (Bersezio et al. 2004; Bini
148 et al. 2004; Bini 1997; Bini and Zuccoli 2001, 2004), sitting above a regional stratigraphic boundary attributed to 0.89
149 Ma ("Red" surface, Muttoni et al. 2003; Scardia et al. 2006, 2012). After retreat of the LGM Alpine glaciers, post-
150 glacial isostatic and tectonic uplift and climate-driven increase of riverine discharges induced the entrenchment of the
151 river network, that is at present mostly confined within low-terraces metres to tens of metres below the average
152 altitude of the plain (the so called "Livello Fondamentale della Pianura", Castiglioni and Pellegrini, 2001).

153 The regional hydrostratigraphy of the central Po plain has been outlined by ENI-Regione Lombardia (2002), who
154 identified four Aquifer Groups (labelled with the letters A to D from top to bottom). The middle – upper Pleistocene
155 glacio-fluvial and alluvial aquifer groups (A and B) consist of multilayer aquifers saturated with freshwater (pore-
156 fluids electrical conductivity ranging between 500 μS/cm and 620 μS/cm; Mele et al. 2012) at the distal, Apennine
157 side of the plain and correspond to a single coarse-grained aquifer at the northern Alpine side of the basin, inclusive of
158 the phreatic and of a thick non-saturated zone at the top. Piezometric measurements from public datasets (the
159 groundwater section of SIA, Environmental Information System of the Milan metropolitan city) show that the depth of
160 the water table becomes shallow from North to South, from a depth of tens of meters to a few meters.

161 The lower Pleistocene – upper Pliocene marine to transitional aquifer groups (C and D) are confined to semi-
162 confined, the regional aquicludes being represented by the fine-grained sediments of shallow marine to distal alluvial
163 plain environment. Connate, high-density and salty pore waters represent a typical feature of the deepest aquifers

(group D). These marine waters, trapped at the bottom of the basin during late Messinian (Conti et al. 2000), rarely rise into the overlying transitional Group C (ENI-Regione Lombardia, 2002) that recurrently contains brackish waters. Uprising of these waters to shallow depths, at the southern side of the Po basin, is due to Apennine thrust faults and fault propagation folds.

This broadly summarised picture suggests the largest scale targets for the resistivity prospection along the North-South traverse across the basin: 1) the top of the highly conductive, fine-grained lower Pleistocene to Mio-Pliocene marine substratum, saturated by salt to brackish waters, which is uplifted and deformed by Apennine fault propagation folds; 2) the lower p.p. and middle Pleistocene syn-tectonic, folded and faulted clastic wedges, onlapping and downlapping the regional erosional unconformity that truncates the underlying marine sediments; the fresh/brackish water interface is contained in the lower part of this resistive succession 3) the middle p.p. – upper Pleistocene highly resistive, coarsening upwards clastic alluvial sequences, which rest on the whole above a regional unconformity and host the S-dipping phreatic surface in the uppermost stratigraphic units.

3. METHODOLOGY AND PRESENTATION OF THE DATA-SET

3.1. GENERALITY OF VES SOUNDING AND MODELLING

A VES consists of a sequence of measurements of apparent electrical resistivity (ρ_{app}) with in-line, four-electrode array, coupled with the ground surface (Keller and Firschknecht 1966; Reynolds 2011). From the flowing current intensity injected through two current electrodes, the measured potential difference between two potential electrodes and a geometrical factor, which depends on the separation of current and potential electrodes and the general scheme of the array, ρ_{app} is computed. For a VES, consecutive measurements of ρ_{app} are collected by increasing the separation between the current and potential electrodes. Doing so, the measured electrical field is sensitive to an increasing volume of subsoil and, therefore, ρ_{app} is influenced by the resistivity distribution at increasing depths (Fig. 2).

Assuming no lateral resistivity transition (1-D assumption) and electrically homogeneous layers, numerical modelling of ρ_{app} is aimed to compute 1-D resistivity-versus-depth profiles that best fit the experimental data. This goal is obtained with inversion methods that, using resistivity and thickness of electrolayers as model parameters, minimize the root mean square relative error (RMS) between the observed and the modelled apparent resistivity. In this paper inversion is performed with the program RES1D (Loke 2001) which is based on a damped, non-linear least-

squares optimization method (Lines and Treitel 1984) and on the "linear digital filter" method (Koefoed 1979) for the forward modelling.

3.2. VES DATA-SET AND FORMER RESULTS AT THE LOCAL-SCALE

The data-set used in this work refers, in part, to the geophysical acquisition campaigns carried out from 2007 to 2012 in three small key-areas (Fig. 1). The general results of these experiments were briefly summarized in the introduction of this paper and are discussed in details by Bersezio et al. (2007) and by Mele et al. (2010; 2012, 2013, 2015).

At these sites, VES exploration yielded quasi-3D information about subsurface with a high horizontal data density, comparable with the characteristic scale lengths of the alluvial depositional systems. The VES clusters were located, from North to South, at three hinge zones in the geological architecture of the basin (Fig. 1):

1) the Northern hinge between the uplifted middle-late Pleistocene proximal glacio-fluvial sandur and the central to southern distal alluvial depositional systems, where the thick freshwater phreatic aquifer group splits into phreatic and semiconfined aquifer systems (Cassano d'Adda-Pozzuolo Martesana cluster, 24 VES; Mele et al. 2015);
2) the central area corresponding to the Lodi synformal depocentre of the Pleistocene clastic wedges, which host freshwater into semi-confined to confined aquifer groups (Lodi Vecchio cluster, 89 VES; Bersezio et al. 2007; Mele et al. 2012);
3) the Southern area where Apennine tectonics affected the Pleistocene sediments, uplifting and locally exhuming the marine sequences, logged by high-conductive brackish to salt-waters and associated to local geothermal anomalies (Casalpusterlengo-Zorlesco cluster, 36 VES; Mele et al. 2013).

Apparent resistivity data were acquired with a four-channel PASI 16G georesistivity-meter and Schlumberger array. Using a maximum half-spacing (i.e. half the distance between the current electrodes) equal to 300 m (Lodi Vecchio and Cassano d'Adda-Pozzuolo Martesana cluster) and to 500 m (Casalpusterlengo-Zorlesco cluster), we explored the upper portion of the alluvial stratigraphy: 1-D resistivity-versus-depth profiles obtained after complete curve matching yielded an estimated maximum depth respectively of 100 m and 250 m bgs. Notice that the maximum current intensity injected into the Earth to obtain reliable data was of the order of almost 600 mA.

The purpose of scaling-up the electrostratigraphic analysis to the regional scale requires a larger investigation depth than that of the former exploration campaigns, in order to reach the deepest Quaternary succession.

To do so, we integrated the available data-set with 15 VES, which were performed with the same instrumental setting and were located in-between and partially overlying the three mentioned VES clusters, from the northern deeply weathered Pleistocene terraces to the southern present day Po valley. The entire data-set has been acquired at the top surface of the uppermost morphological terrace, skipping the entrenched post-Glacial to Holocene valleys (Fig.1), having care to investigate comparable stratigraphic sequences at every site. The separation between VES acquisition station ranges from 1.5 km to 5.5 km; relatively large half-spacings (up to 1,000 m) permitted deep investigation. The numerical interpretation yielded 1-D resistivity-versus-depth profiles down to an estimated maximum depth of 450 m bgs. The RMS obtained after inversion of the VES apparent resistivity curves with RES1D was lower than 2.8% with up to 11 electro-layers.

3.3. 1-D MODELLING AND REGIONAL HIERARCHIC ELECTROSTRATIGRAPHY

The specific basin-scale application along the North-South cross-section of the Po basin was performed with a two-step, geophysical and geological procedure to manage 1-D resistivity-versus-depth profiles.

At the first step, we focused on the number and on the polarity of the interfaces, as both these properties concur in the identification of the local vertical electrostratigraphic sequence, which in turn controls the shape of the apparent resistivity field curves. This approach was implemented by inverse modelling of VES field curves, with the tools described in the previous section, and by evaluating the numerical fit between experimental and modelled data as a function of the number and the polarity of interfaces at each VES. In Fig. 3 is shown an illustrative example of the multiple interpretation with equivalent electrostratigraphies at VES T7 (location in Fig. 1), and the corresponding values of RMS error, obtained for three- to seven-layer models. At the end of this step, for each VES we considered satisfactory the resistivity-versus-depth profile obtained when no appreciable decrease in RMS error is generated by a focused addition of an electrolayer. In particular, an additional layer was inserted with the specific aim to reduce the misfit of the most loosely fitted parts of the field curve (see caption of Fig. 3). This procedure can be illustrated by means of the example in Fig. 3. The addition of layers for the models with a number of layers up to 6 is aimed to the improvement of the field-curve fit for long half-spacing of the current dipoles. On the other hand, the decrease in RMS error between six- and seven-layer models is due to the addition of a low-order interface (see later for details) at shallow depth for the best fitting of the initial part of the field curve (half-spacing less than 30 m), which shows some oscillations, symptoms of fall of 1-D assumption for possible shallow lateral heterogeneities.

Of course, the interpretation of a single VES is affected by equivalence, i.e., multiple, layered structures with different thicknesses and resistivities might fit the field data with a similar RMS error. Geoelectrical equivalence is still an open scientific problem and it could be reduced by independent data (for example, the exact depth of calibrated interfaces inferred from borehole logs) or could be managed with different techniques of inversion in case of multiple data-set (e.g., laterally constrained inversion; Auken et al. 2005; Christiansen et al. 2007). This important issue is beyond the scope of this paper and here is considered in an indirect way only, through the check performed during the following step of the procedure.

At the second step, we traced the interfaces between adjacent VES stations along the North-South cross-section, according to their polarity, i.e. the mentioned R-C and/or C-R patterns, and to the horizontal trend of variation of the local electrostratigraphy (Fig. 4). We conducted a critical evaluation of the validity of the subsurface geometries in terms of hierarchic electrostratigraphic interfaces and EsUs by matching non-contradiction, internal consistency, simplicity and likelihood criteria. At this stage. the electrostratigraphic results obtained at the three small-scale key-sectors were incorporated(see section 3.2, Fig. 1 and references therein). At the end of this analysis, we eventually re-evaluated the equivalent models obtained at step 1 in order to choose those which provide the identification of the major order electrostratigraphic interfaces and the smoothest geometries.

The resulting cross-section is presented in Fig. 5 and the detailed description of EsUs can be found in Tab.1. In the cross-section we represent the VES with the largest exploration depth (>100 m bgs), complemented by a limited number of shallow (<100 m bgs) resistivity-versus-depth profiles. Considering the quasi-3D results at the three fine-scale key-sectors (Fig. 1; see references therein) it should be noted that, while the regional cross-section shows EsUs in 2D, the 3-D distribution of VES stations across the basin and the adopted electrostratigraphic criteria allow to consider EsUs as the expression of 3-D electrostratigraphic bodies.

The calibration of the cross-section has been obtained at the three key-sectors using: 1) correlation panels from lithological logs (boreholes; see Fig. 1 for location); 2) short and long normal resistivity logs from a deep hydrocarbon well (within the Casalpusterlengo-Zorlesco cluster); 3) the electrical conductivity of groundwater and 4) the depth of the water table in the LFP. This matter is presented and discussed in details by Bersezio et al. (2007) and Mele et al. (2010, 2012, 2013, 2015). In the cross-section of Fig. 5 we show, as a reference, a limited number of litho-textural logs from water wells (less than 170 m bgs) to facilitate comparisons with the regional subsurface stratigraphy.

At the regional scale portrayed by the resistivity cross-section, four laterally persistent, resistivity discontinuities have been mapped. They were informally named S1 to S4 from top to bottom (Fig. 5; see also the discussion of the results in the following section). In the hierarchic electrostratigraphic architecture we assigned them the highest-rank (1st order). According to the polarity, lateral persistence and vertical resistivity trends, S1 to S4 1st order electrostratigraphic discontinuities bound five highest-rank Groups of EsUs, numbered in increasing order downwards from the ground surface from Group 1 to 5 (Tab. 1; Fig. 5). The electrical resistivity ranges estimated for the EsUs forming each Group are comparable with those previously obtained at the key-sectors and are listed in Tab. 1.

Intermediate-rank discontinuities (2nd order) delimit individual 2nd-order EsUs preserving the polarity (C-R or R-C) between adjacent and overlapping units (Fig. 4 and Fig. 5). The lowest-rank interfaces (3rd order) represent internal heterogeneities within the individual EsUs, i.e. they bound sub-volumes within the EsUs showing the lowest variation of electric resistivity (electrical homogeneity criteria; Fig. 4). This is the rank of the individual electrolayers in the 1-D interpretation of a VES. In 2-D and 3-D, at regional scale, their lateral continuity and overall geometry are highly uncertain, in particular for lense-shaped units detected in single VES (for example, in T6 and T8; Fig. 5), due to the intrinsic limit of vertical resolution at increasing depth for VES interpretation. Hence only their inferred boundaries are drawn in the regional cross-section (Fig. 5, dotted lines) and they are not considered in Tab.1. To resolve the third order resistivity heterogeneity at shallow depth, more detailed surveys, like 2-D resistivity imaging and Ground Penetrating Radar (Mele et al. 2012), are necessary, and should be applied to a much finer scale than the basin-wide scale. On the other hand, at greater depth, the third order units could be resolved only by independent data

4. DISCUSSION OF RESULTS

4.1. THE REGIONAL RESISTIVITY CROSS-SECTION

The resistivity cross-section is represented in Fig. 5 using 23 selected resistivity-versus-depth profiles. The five 1st order groups of EsUs describe an overall, large-scale, upwards increasing trend of electrical resistivity that is associated to important changes in the staking patterns of the 2nd order EsUs. This pattern compares to the regional regressive trend from marine sediments (initially and still partly logged by saltwater) to the coarsest-grained prograding glacio-fluvial units (freshwater logged) known from literature, and summarised in section 2. Vertical and horizontal internal resistivity trends do exist also within the Groups of EsUs (Fig. 6a and b respectively). The observed vertical resistivity trends are of three types: upwards increasing, upwards decreasing and stationary. In the

302 stratigraphic setting of the study area these trends mimic respectively the typical coarsening/thickening,
303 fining/thinning and stationary stacking pattern trends of sedimentary units. Also southward and northward horizontal
304 trends of resistivity could be detected and traced within and across the 2nd order EsUs and 1st order Groups (Fig. 5 and
305 6b). Hence, Fig. 5, Fig. 6 and Tab. 1 permit to read and interpret the combination of the array of electrostratigraphic
306 features that could be detected: the geometry of the electrostratigraphic units of the 1st and 2nd order and of their
307 boundaries, the spatial assemblage of the EsUs and their mutual relations, the vertical and horizontal resistivity trends
308 within the units and through their assemblage.
309 Considering the calibration procedure which was adopted (section 3.3), the resistivity field responds to the
310 heterogeneous distribution of the litho-textural properties of the sedimentary bodies showing the strong analogy of the
311 reconstructed electrostratigraphic architecture with the known geological and hydrogeological/hydrogeochemical
312 features, which was described in section 2. This permits to interpret the electrostratigraphic cross-section in terms of
313 subsurface geology, including the simplest and most obvious tectonic and stratigraphic features and the relative
314 chronology from which they derive. At last the stratigraphic interpretation can also be transposed to a
315 hydrostratigraphic architecture, which is one of the expected applications of this implementation of the
316 electrostratigraphic prospecting method. The stack of 1st order Groups of EsUs can be summarized as follows,
317 descending from the ground surface.
318 Group 1 (red-pink-white colours in Fig. 5) is the shallowest and therefore the best resolved EsU, which justifies a
319 more detailed interpretation compared to the underlying units. It is bounded at the base by electrical discontinuity S1
320 and consists of a stack of interfingered, wedge-shaped and southward-dipping, resistive and conductive EsUs,
321 delimited by 2nd order surfaces. These EsUs show a decreasing tilt toward South and an apparent downward
322 termination above the gently curved and southwards-dipping S1 and/or above one another. These features mimic the
323 typical depositional geometry of a downlapping, progradational stacking pattern, as it might be interpreted in terms of
324 physical stratigraphy from a seismic line or from a borehole stratigraphic correlation panel. Between VES T16 and
325 T22 (Fig. 5), acquired in the area of the southern Casalpusterlengo and Zorlesco structural highs (Desio 1965;
326 Cremaschi 1987; Bersezio et al. 2010), the basal resistive EsU of Group 1 shows an upward curvature, mimicking a
327 folded synformal-antiformal pattern, while the overlaying EsUs follow up-section without bending. In geological
328 terms we could interpret this electrostratigraphic pattern as the image of the relationships between less deformed
329 sediments sitting above a folded stratigraphic unit. Highly uncertain third order resistivity interfaces are mapped

within the resistive EsUs, aiming to highlight the lateral resistivity transitions at the horizontal scale of tens of kilometres (Fig. 6b). On the opposite, conductive units are tabular, quite homogeneous and show northward stepping terminations, mimicking a retrogradational stacking pattern of fine grained, transgressive, depositional packages, if compared to the southward "prograding" pattern of the resistive 2nd order EsUs. The overall electrostratigraphic sequence of Group 1 shows small-scale, upward-decreasing resistivity cycles (see VES T3, T6, and T9 in Fig. 5 and Fig. 6a) that are delimitated at their top by the surface topography. The average modelled thickness of this group is about 50 m along the central and the southern part of traverse, while it thickens to North up to about 100 m (T1 in Fig. 5).

Group 2 (dark and light yellow colours in Fig. 5) sits above electrostratigraphic discontinuity S2 and consists of a couple of EsUs revealed by VES between T7 and T20, in the region of the Lodi synformal depocentre adjacent to the North and to the South the Casalpusterlengo – Zorlesco structural highs. Group 2 depicts a large, upward decreasing resistivity trend, characterized by a resistive EsU at the base and a conductive EsU at the top (VES T12 in Fig. 5). Both units form two lenses which wedge-out northwards and southwards, where S2 reaches its shallowest depth and joins S1 from below. In geological terms, these features could be interpreted as folding and subsequent erosional truncation (S1 truncating S2 and Group 2) of a fining-upwards large-scale sedimentary sequence. The geometry of the EsUs, their mutual relationships and the relations between Group 2 and the underlying Groups suggest progressive southwards and northwards onlaps of Group 2 EsUs onto the top of Groups 3 and 4, as it is apparent in the vicinity of the Casalpusterlengo and Zorlesco structural high (T16 – T22, Fig. 5).

Group 3 (dark and light green colours in Fig. 5) consists of curved EsUs lying above electrostratigraphic discontinuity S3, forming one large-scale upwards-decreasing resistivity cycle (Fig. 6a). The lower resistive EsU shows a lateral resistivity decrease from North to South, i.e. toward the Lodi synformal depocentre that reverses close to the Casalpusterlengo and Zorlesco structural highs (Fig. 6b). Southwards of VES T10, the lower resistive EsU looks to be uplifted and sealed by the upper conductive EsU, plunging toward South, whereas it is truncated by S2 (Fig. 5, complete truncation of Group 3 occurs between VES T13 and T16). Two resistive lenses tens of meters thick are interpreted with some uncertainty at VES T6 and T8 within the upper conductive EsU.

Group 4 (dark - light blue and cyan colours in Fig. 5) is a widespread conductive interval which embeds resistive wedges and lenses. The overall geometry of Group 4 is comparable to kilometre-scale folds, forming a synform (North) – antiform (South) pair. The buried antiformal bend develops below the surface expression of the

Casalpusterlengo – Zorlesco structural high. In the northern part of the electrostratigraphic cross-section (VES T1 - T4; Fig. 5), a South-dipping, wedge-shaped, resistive EsU is present in the core of Group 4. In correspondence of the Casalpusterlengo and Zorlesco structural high, a curved, lens-shaped, resistive EsU is mapped (VES T19 - T23; Fig. 5). Both these wedge-shaped EsUs thin and wedge-out towards the central synform that broadly corresponds to the Lodi synformal depocentre. Group 4 reaches its maximum modelled thickness (about 300 m) towards the northern end of the cross-section. The stacking of the EsUs gives origin to a lower trend of increasing resistivity, that is followed upwards by an opposite trend above the resistive lenses (Fig. 6a). A trend of decreasing resistivity can be observed from North to South, leaving from the northern resistive lens-shaped EsU (Fig. 6b).

Group 5 (grey colour in Fig. 5) consists of extremely-high conductive EsUs, revealed in the central and southern parts of the electrostratigraphic cross-section. These EsUs could be reached either at the sites where the deepest investigation depth was attained (between T6 and T9, T15; Fig. 5) or where they are uplifted close to the ground surface (T16 – T21, Fig. 5; Casalpusterlengo structural high area). The extremely-high conductive EsUs correspond to the core of the antiformal bend portrayed in the most uplifted sector of the Casalpusterlengo structural high. These features might be interpreted, in geological terms, as the result of synclinal-anticlinal folding of the marine, highly conductive substratum of the Pleistocene clastic sequence.

4.2. HYDROSTRATIGRAPHIC INTERPRETATION

The regional electrostratigraphy of the Po plain in central Lombardy shows a general upwards-increasing resistivity trend. This is in accordance with the regional, coarsening-upwards depositional trend, from the lowermost fine-grained, well-bedded and conductive units of the (Mio)-Plio-Pleistocene marine-to-transitional depositional systems to the progressively more coarse-grained, massive and resistive fluvial and glacio-fluvial depositional systems of the Middle–Late Pleistocene (Ghielmi et al. 2013; Ori 1993). Pore-water chemistry and saturation changes contribute to this pattern, salt- to brackish water being confined to the deepest Group 5 and to part of the overlying Group 4, while freshwater saturates Group 3, Group 2 and the lower part of Group 1, which contains the phreatic surface (Fig. 5; compare with the fresh-saltwater interface depth reported from ENI oil wells in ENI-Regione Lombardia, 2002).

If these interpretations are correct, the resistivity image of Fig. 5 and Fig. 6 represents a proxy of the hydrostratigraphic architecture, showing that the Northern, single, large-scale and thick aquifer (about North of T6 in

Fig. 5) splits progressively southwards into thin, coupled, aquifers and aquitards (South of T6 in Fig. 5; compare with the hydrostratigraphic cross-sections in Bersezio et al. 2004, 2010 and ENI-Regione Lombardia 2002).

At increasing depth below Group 1, the resolution decreases and a progressively less detailed image must be interpreted. Freshwater-logged, regressive aquifer systems, partly or totally confined by the intervening transgressive fine-grained aquitard/aquiclude systems are confidently interpreted from the stack of folded resistive and conductive EsUs shown by the electrostratigraphic image of Groups 3 and 4 below S2.

Below S3 the most conductive 1st order Groups 4 and 5 occur. Both are uplifted close to ground surface by the Casalpusterlengo ramp-fold at the southern end of the cross-section, as it is confirmed by borehole stratigraphy at Casalpusterlengo-Zorlesco (Bersezio et al. 2010) and outcrop geology at the neighbouring San Colombano relief (Desio 1965; Anfossi et al. 1971; Boni, 1967; Bersezio et al. 2016). The top boundary of the deepest 1st order Group 5 (the most conductive unit) most plausibly represents the salt/brackish water interface. Inside Group 4, lens-shaped freshwater aquifers are confined within the marine aquitard, conductive fines with a repetition of the brackish/freshwater interface.

4.3. GENERAL REMARKS ON ELECTROSTRATIGRAPHY

The Po Plain electrostratigraphic cross-section shows that the hierarchically arranged electrostratigraphic units (EsUs, EsUs Groups and the corresponding resistivity boundaries) clearly have different expression, extension and modelled thicknesses, i.e. different sizes. Electrical resistivity can be considered as an equivalent volume-averaged physical property between the “shale”-dominated conduction volumes and the “electrolytic”-dominated conduction volumes (Mele et al. 2012, 2014, 2015), and therefore it bears extremely different geological and hydrostratigraphic information for subsurface reconstruction.

This is important in terms of the prominent geological controlling factors on subsurface electrical conduction because it directly implies that when observed regardless of their physical scale, the resistivity volumes appear similar to one another, because the corresponding stratigraphic units are characterized by comparable styles of propagation of the internal heterogeneities affecting the bulk electrical conduction.

At the fine-scale, typically investigated by high-resolution borehole logs, laboratory experiments (Inzoli and Giudici 2015; Mele et al. 2014) or ground-based DC methods focused to the near-surface (Bersezio et al. 2007), the transition between sediment volumes with homogeneous electrical properties mainly occurs at definite physical

414 interfaces. This is the case of sedimentary facies transition, corresponding to a resistivity contrast whose magnitude is
415 linked to the textural parameters concurring to the variation.

416 On the contrary, when electrical resistivity ground-based methods are used to explore large volumes of stratified
417 sediments, the electrical equivalence restricts the size of the vertical heterogeneities that can be resolved. As a
418 consequence, the interpreter is forced to consider the vertical sequences of thin strata at depth as a single electrically
419 macro-anisotropic entity (Christensen 2000). In this way the sediments are depicted as a function of the resolving
420 power of the method, which acts as a low-pass filter with respect to the vertical wavenumber components of electrical
421 resistivity, enabling to detect only low-wavenumber resistivity variations related to the sediments' nested hierarchy
422 that emerged at different depths (and physical scales) of observation.

423

424 ## 5. CONCLUSIONS

425 A 72-kilometer-long cross-section, based on electrostratigraphic correlation of resistivity-versus-depth profiles
426 obtained by VES soundings, has been portrayed across the Po plain in central Lombardy, down to 300 m below sea-
427 level, to investigate the architecture of the Quaternary fill of the Po Apennine foreland basin.

428 The test shows that:

429 1) the survey permits to depict the subsurface geology of the uppermost 400 m of the basin stratigraphy. In the
430 densely populated alluvial plains of the world, this depth interval is of paramount relevance for many
431 applications (e.g. hydrogeology, geothermal exploitation, quarrying and digging, subsidence problems and so
432 on), but it is often poorly understood yet. In the case of the Po plain, the new generation of electrostratigraphic
433 cross-sections permits to start closing the gap between deep seismic images by the oil-industry, that are still
434 poorly oriented to show in detail the shallow geology, and the very shallow water wells and borehole-derived
435 stratigraphic reconstructions (Cassano et al. 1986; ENI-Regione Lombardia 2002; Fantoni et al. 2004; Ghielmi
436 et al. 2013; Pieri and Groppi 1981);
437 2) The cross-section has been obtained thanks to the refinement of the concepts and methodology of
438 "electrostratigraphy", after a set of studies dedicated to improve and test the detailed resistivity imaging of the
439 Po basin subsurface at the local scale. The wide physical scale of the experiment is relevant for this test. As a
440 matter of fact, such a large volume in a tightly constrained tectono-sedimentary framework involves large-scale
441 changes of the prominent controlling factors on electrical resistivity (i.e. gradual to sharp changes of texture

and composition of the investigated sediments and rocks, changing water saturation, changing underground water chemistry and temperatures, gradual to abrupt changes of shape, bedding styles and stacking patterns of the sedimentary bodies, pinch-outs, erosional unconformities, folds and tectonic dips and so on). These remarks now permit to conclude that electrostratigraphic units can represent a category of geophysical-stratigraphic units, comparable to seismic units or to some of the traditional categories like allostratigraphic or lithostratigraphic units (NASC 2005). Provided that the resistivity method permits to interpret the sediments as a function of the resolving power, and that the resolution lowers with depth, the survey demonstrates that: i) EsUs have boundaries, that are detectable resistivity interfaces preserving the polarity wherever they exist; ii) EsUs are formed by sediment/rock volumes showing a relatively narrow range of resistivity values, admitting lateral and vertical trends (upwards and/or laterally increasing, decreasing or stationary); when pore fluids' chemistry is constant, the latter plausibly relate directly to the stacking pattern of sedimentary bedsets (i.e. fining/coarsening, thinning/thickening and stationary trends); iii) EsUs are hierarchically arranged, the basic unit being the EsU that contains sub-units (1-D electrolayers, hardly traceable at regional scale) and can be clustered into Groups of EsUs; iv) they are related to some fundamental features of the stratigraphic sequences (i.e. the composition of sediments, the net-to-gross ratio, the fluid chemistry and saturation, hence they can be calibrated to the known local stratigraphic and structural settings, rather than to individual borehole data-points); v) they have external geometry and mutual relationships, so the calibrated electrostratigraphic picture can be interpreted, with the proper caution, in terms of geological architecture, relative chronology and evolution;

3) The electrostratigraphic cross-section shows the most relevant stratigraphic and tectonic features of the Quaternary fill of the central Po plain, along a traverse sitting on the structural fronts of both Alps and Apennines, in satisfactory agreement with the available literature. A synthetic list of such features includes: i) the frontal salient of the Northern Apennines, represented by the Casalpusterlengo thrust-propagation anticline, that folds the ESUs of Groups 4 and 5, the deepest, which might correspond to the (Mio)-Pliocene - Calabrian marine to transitional fine-grained succession and contain the present-day saltwater and brackish-freshwater interfaces; ii) the on-lapping, off-lapping and truncated EsUs of Group 3, which could correspond to the Calabrian alluvial to littoral regressive – transgressive cycle. Group 3 is interpreted as affected by ongoing syn- to post-depositional folding; iii) the fill of the Lodi synformal depocentre, i.e. Group 2, that is interpreted as the

expression of the Calabrian – middle Pleistocene distal alluvial and glacio-fluvial sequence, related to the Verbano and Lario amphitheatres. The electrostratigraphic image permits to infer that this Group underwent syn-depositional folding and subsequent truncation to the South (Casalpusterlengo, Zorlesco and related thrust-propagation folds) concurrent with uplift and erosion at the northern side, that sits above the Southalpine thrusts at that time involved as the peripheral bulge of the Apennines, iv) the prograding – retrograding EsUs of Group 1, the shallowest one, sitting on an "electrical unconformity" (1st order surface S1) that truncates the underlying groups both on the crest of the Casalpusterlengo anticline (South) and on the uplifted ramp to the North. This Group, that contains the phreatic surface, is calibrated to the Middle – Late Pleistocene glacio-fluvial to post-glacial alluvial sediments. The uppermost EsU seals unconformably the southernmost tectonic structures. Within this group, the geophysical resolution which could be attained at shallow depth, permits to recognize at least three cycles of resistive and coarse-grained sediments prograding from North to South above more conductive, fine-grained deposits, which are finally cut and filled by the ESUs hosted into the post-Glacial to Holocene Po terraced valley. Group 1 ESUs might represent the major Middle – Late Pleistocene glacial advance and retreat cycles of the Lario amphitheatre (Binago-Specola, Besnate, and Cantù/LGM glaciations; Bini et al. 2004). At last, it might be observed that the interpretation of the electrostratigraphic cross-section in terms of geological evolution provides an additional validation tool of the geophysical image, by comparison with the current geological reconstructions, if available.

4) The electrostratigraphic image is a picture of the resistivity distribution that can be interpreted in terms of petrophysical properties of the subsurface succession, like hydraulic conductivity, hence it might represent a good proxy of the hydrostratigraphic structure of the central Po plain. Fig. 5 shows that Group 4 represents the basal confining layer that sustains the confined aquifers represented by the overlying EsUs of Groups 3 and 2. Group 4 also contains large-scale isolated lenticular aquifer systems and the related multiple base of the freshwater aquifers. The fine-grained top EsUs of Groups 3 and 2 represent the aquitard-aquiclude layers which confine the aquifers hosted by Group 1. The top EsUs of Group 1 contain the piezometric surface and the related flowing wells, that form a well-known E-W trending belt at the northern side of the Po plain.

5) The DC survey complemented with the electrostratigraphic interpretation and calibration yields promising results, at low-cost and with almost no environmental impact, concerning that depth range which often escapes the other geophysical techniques. The application to a regional case study, which is typical of the very common

and diffuse geological setting of an alluvial plain within a foreland basin, suggests that this approach could yield good results in many other regions, assuming a general validity. In any case, in order to obtain plausible pictures and interpretations and to reduce the uncertainties on the final reconstruction, the geoelectrical results must always be integrated with the existing geological knowledge and with any other independent geophysical prospecting technique.

6. ACKNOWLEDGMENTS

The Authors would like to thank Dr Silvia Inzoli, Dr Emmanuele Cavalli, Dr Alessandro Comunian for their constructive comments and suggestions and Micol Bussolesi, Santiago Pozzoni, Alessio Brusamolino and Stefano Maggio for their helpful support during field data acquisition and data–management and processing. We acknowledge three anonymous Reviewers for their useful suggestions.

7. REFERENCES

Alfano L, Mancuso M (1996) Sull'applicabilità del metodo dipolare-dipolare continuo nelle ricerche idriche a media profondità in aree di pianura. Acque Sotterranee, 13:61-71.

Anfossi G, Desio A, Gelati R, Laureri S, Petrucci F, Venzo S (1971) Note illustrative della carta Geologica d'Italia alla scala 1:100.000. Foglio 60 – Piacenza. 37 pp.. Servizio Geologico d'Italia, Roma.

Auken E, Christiansen AV, Jacobsen BH, Foged N, Sørensen KI (2005) Piecewise 1D laterally constrained inversion of resistivity data. Geophys Prospect 53:497-506. doi: 10.1111/j.1365-2478.2005.00486.x

Baio M, Bersezio R, Bini A (2004) Assetto geologico della successione Quaternaria nel sottosuolo tra Melegnano e Piacenza. Il Quaternario (It J Quat Sc) 17: 355 – 359.

Bersezio R, Giudici M, Mele M (2007) Combining sedimentological and geophysical data for high-resolution 3-D mapping of fluvial architectural elements in the Quaternary Po plain (Italy). Sediment Geol 202:230-248. doi:10.1016/j.sedgeo.2007.05.002

Bersezio R, Fantoni R, Pessina C (2001) L'assetto strutturale del margine sudalpino-padano: contributo alla conoscenza del sottosuolo nel settore Bergamasco. Geologia Insubrica 671:81-94.

524 Bersezio R, Pavia F, Baio M, Bini A, Felletti F, Rodondi C (2004) Aquifer architecture of the Quaternary alluvial
525 succession of the southern Lambro basin (Lombardy, Italy). Il Quaternario (It J Quat Sc) 17:361-378

526 Bersezio R, Cavalli E & Cantone M (2010) Aquifer building and Apennine tectonics in a Quaternary foreland: the
527 southernmost Lodi plain of Lombardy. Mem. Descr.C arta Geol. d'It., XC: 21-30, Roma.

528 Bersezio R, Zuffetti C, Cavalli E, Baio M, Cantone M, Inzoli S, Mele M, Pavia F, Rigato V, Rusnighi Y, Rodondi
529 C, Sozzi S (2016) The Quaternary North-Apennine tectonics recorded in the Po basin: stratigraphic and
530 geomorphological evidences along a N-S traverse in Lombardy (Italy). Geophys Res Abstr, EGU 2016-9228.

531 Bigi G, Cosentino D, Parotto M, Sartori D, Scandone P (1990) Structural model of Italy. Progetto Finalizzato
532 Geodinamica CNR, 114, 3. SELCA, Firenze.

533 Bini A (1997) Problems and methodologies in the study of Quaternary deposits of the Southern side of the Alps.
534 Geologia Insubrica 2:11-20

535 Bini A, Zuccoli L (2001) Geologia di sottosuolo della Valle Olona tra Malnate e Lonate Ceppino (Varese).
536 Geologia Insubrica 6: 19-63.

537 Bini A, Zuccoli L (2004) Glacial history of the southren side of the Central Alps. In: Quaternary Glaciations –
538 Extent and Chronology, J.Ehlers and P.L. Gibbard Editors, 195 – 200. Elsevier, Amsterdam

539 Bini A, Strini A, Violanti D, Zuccoli L (2004) Geologia di sottosuolo dell'alta pianura a NE di Milano Il
540 Quaternario (It J Quat Sc) 17:343-354.

541 Binley A, Cassiani G, Deiana R (2010) Hydrogeophysics: opportunities and challenges. Bollettino di Geofisica
542 Teorica ed Applicata 51:267-284

543 Boni (1967) Note Illustrative della Carta Geologica d'Italia alla scala 1:100.000. Foglio 59, Pavia. 69 pp.. Servizio
544 Geologico d'Italia, Roma.

545 Bresciani I, Perotti C. (2014) An active deformation structure in the Po plain (N Italy): the Romanengo anticline.
546 Tectonics 33:2059-2076. doi: 10.1002/2013TC003422.

547 Bridge JS, Hyndman DS (2004) Aquifer characterization. In: Bridge, J.S., Hyndman, D.W. (ed) Aquifer
548 Characterization. SEPM Spec Publ 80:1-2.

549 Burrato P, Ciucci F, Valensise G. (2003) An inventory of river anomalies in the Po plian, Northern Italy: evidence
550 for active blind thrust faulting. Annals of Geophysics, 46: 865-882.

551 Carminati E, Martinelli G, Severi P (2003) Influence of glacial cycles and tectonics on natural subsidence in the Po
552 plain (Northern Italy): insights from 14C ages. Geochem Geophys Geosyst 4:1082-1096. doi:10.1029/2002GC000481

553 Cassano E, Anelli A, Fichera R, Cappelli V (1986) Pianura Padana: interpretazione integrata di dati geologici e
554 geofisici. Proceedings 73° meeting of the Italian Geological Society, 27 pp., Rome.

555 Castiglioni GB, Pellegrini GB (2001) Note illustrative della Carta Geomorfologica della Pianura Padana.
556 Supplementi di Geografia Fisica e Dinamica Quaternaria IV. 207 pp., Comitato Glaciologico Italiano, Torino.

557 Cavalli, E. 2011. Messa a punto di una metodologia per la modellazione tridimensionale e multiscala
558 dell'idrostratigrafia, su base GIS. PhD thesis, 250 pp., Università degli Studi di Milano.

559 Christensen NB (2000) Difficulties in determining electrical anisotropy in subsurface investigations. Geophys
560 Prospect 48:1-19. doi:10.1046/j.1365-2478.2000.00174.x

561 Christiansen AV, Auken E, Foged N, Sørensen KI (2007) Mutually and laterally constrained inversion of CVES
562 and TEM data: a case study. Near Surface Geophys 5(2); 115-123.

563 Conti A, Sacchi E, Chiarle M, Martinelli G, Zuppi GM (2000). Geochemistry of the formation waters in the Po
564 plain (Northern Italy): an overview. Appl Geochem 15:51-65. doi:10.1016/s0883-2927(99)00016-5

565 Cremaschi M (1987) Paleosols and vetusols in the central Po plain (Northern Italy). Collana Studi Ric Territ, 28,
566 306 pp., UNICOPLI, Milano

567 Desio A (1965) I rilievi isolati della pianura Lombarda ed i movimenti tettonici del Quaternario. Rendiconti
568 dell'Istituto Lombardo 99:881-894.

569 ENI-Regione Lombardia (2002) Geologia degli acquiferi padani della Regione Lombardia. 130 pp, SELCA,
570 Firenze

571 Fantoni R, Franciosi R (2010) Tectono-sedimentary setting of the Po plain and Adriatic foreland. R. Rend. Fis.
572 Acc. Lincei21 (suppl. 1):197- 209. doi:10.1007/s12210-010-0102-4

573 Fantoni R, Massari FMinervini M, Rogledi S, Rossi M (2001) Il Messiniano del margine Sudalpino-Padano:
574 relazioni tra contesto strutturale e stratigrafico-deposizionale. Geologia Insubrica 6:95-104.

575 Fantoni R, Bersezio R, Forcella F (2004) Alpine structure and deformation chronology at the Southern Alps Po
576 plain border in Lombardy. Bollettino della Società Geologica Italiana 123: 463-476.

577 Francese R, Giudici M, Schmitt DR, Zaja A (2005) Mapping the geometry of an aquifer system with a high-
578 resolution reflection seismic profile. Geophys Prospect 53:817-828). doi:10.1111/j.1365-2478.2005.00506.x

579 Galloway WE, Sharp JM Jr (1998) Characterizing aquifer heterogeneity within terrigenous clastic depositional
580 systems. In: Fraser G.S. and Davis J.M. (ed) Hydrogeologic models of sedimentary aquifers. SEPM Concepts in
581 Hydrogeology and Environmental Geology 1:85-90. Society for Sedimentary Geology, Tulsa

582 Ghielmi M, Minervini M, Nini C, Rogledi S, Rossi M, Vignolo A (2010) Sedimentary and tectonic evolution in the
583 eastern Po plain and Northern Adriatic sea area from Messinian to Middle Pleistocene (Italy). Rend. Fis. Acc. Lincei
584 21 (suppl. 1):131-166. doi:.1007/s12210-010-0101-5

585 Ghielmi M, Minervini M. Nini C, Rogledi S, Rossi M. (2013) Late Miocene – Middle Pleistocene sequences in the
586 Po plain – Northern Adriatic sea (Italy) the stratigraphic record of modification phases affecting a complex foreland
587 basin. Mar Petrol Geol 42:50-81. doi: 10.1016/j.marpetgeo.2012.11.007

588 Giudici M (2010) Modeling water flow and solute transport in alluvial sediments: scaling and hydrostratigraphy
589 from the hydrological point of view. In: Bersezio R, Amanti M (ed) Proceedings of the Second National Workshop
590 “Multidisciplinary approach for porous aquifer characterization”. Memorie Descrittive della Carta Geologica d’Italia
591 XC:113-120, ISPRA, Roma

592 Giudici M, Mele M, Inzoli S, Comunian A, Bersezio R (2015) The application of hydrogeophysics to study water-
593 based ecosystems services in alluvial plains. First Break 33:55-60.

594 Hubbard SS, Rubin Y (2000) Hydrogeological parameter estimation using geophysical data: a review of selected
595 techniques. J Contam Hydrol 45:3-34. doi:10.1016/S0169-7722(00)00117-0

596 Huggenberger P, Aigner T (1999) Introduction to the special issue on aquifer-sedimentology: problems,
597 perspectives and modern approaches. Sediment Geol 129:179-186. doi:10.1016/S0037-0738(99)00101-3

598 Inzoli S, Giudici M (2015) A comparison between single- and multi-objective optimization to fit spectral induced
599 polarization data from laboratory measurements on alluvial sediments. J Appl Geophys 122:149-158.
600 doi:10.1016/j.jappgeo.2015.09.017.

601 Keller GV, Frischknecht FC (1966) Electrical methods in geophysical prospecting. Pergamon Press, 519 pp.
602 Oxford.

603 Koefoed O (1979) Geosounding principles, 1: resistivity soundings measurements. Elsevier, 276 pp, Amsterdam.

604 Lines LR, Treitel S (1984) A review of least-squares inversion and its application to geophysical problems.
605 Geophys Prospect 32:159-186. doi:10.1111/j.1365-2478.1984.tb00726.x

606 Livio FA, Berlusconi A, Michetti AM, Sileo G, Zerboni A, Trombino L, Cremaschi M, Mueller K, Vittori E,
607 Carcano C, Rogledi S (2009) Active fault-related folding in the epicentral area of the December 25, 1222 (Io=IX
608 MCS) Brescia earthquake (Northern Italy): Seismotectonic implications. Tectonophysics 476:320-335. doi:
609 10.1016/j.tecto.2009.03.019

610 Livio F, Berlusconi A, Zerboni A, Trombino L, Sleo G, Michetti AM, Rodnight H, Spötl C (2014) Progressive
611 offset and surface deformation along a seismogenic blind thrust in the Po Plain foredeep (Southern Alps, Northern
612 Italy). J Geophys Res 119:7701-7721. doi:10.1002/2014JB011112.

613 Loke MH (2001) RES1D ver. 1.00a Beta. 1-D Resistivity, IP and SIP Modeling. www.geotomosoft.com

614 Mele M, Bersezio R, Giudici M, Rusnighi Y, Lupis D. (2012) The architecture of alluvial aquifers: an integrated
615 geological-geophysical methodology for multiscale characterization. Mem. Descr. Carta Geol. D'It., XC: 209-224,
616 Roma.

617 Mele M, Bersezio R, Giudici M (2012) Hydrogeophysical imaging of alluvial aquifers: electrostratigraphic units in
618 the quaternary Po alluvial plain (Italy). Int J Earth Sc 101 (7): 2005-2025. doi:10.1007/s00531-012-0754-7

619 Mele M, Bersezio R, Giudici M, Inzoli S, Cavalli E, Zaja A (2013) Resistivity imaging of Pleistocene alluvial
620 aquifers in a contractional tectonic setting: a case history from the Po plain (Northern Italy). J App Geophys 93:114-
621 126. doi:10.1016/j.jappgeo.2013.03.015.

622 Mele M, Inzoli S, Giudici M, Bersezio R (2014) Relating electrical conduction of alluvial sediments to textural
623 properties and pore-fluid conductivity. Geophys Prospect 62:631-645. doi:10.1111/1365-2478.12102

624 Mele M, Ceresa N, Bersezio R, Giudici M, Inzoli S, Cavalli E (2015) Resolving electrolayers from VES: a
625 contribution from modeling the electrical response of a tightly constrained alluvial stratigraphy. J App Geophys
626 119:25-35. doi: 10.1016/j.jappgeo.2015.05.002.

627 Muttoni G, Carcano C, Garzanti E, Ghielmi M, Piccin A, Pini R, Rogledi S, Sciunnach D (2003) Onset of Major
628 Pleistocene glaciations in the Alps. Geology 31:989-992. doi:10.1130/G19445.1

629 North American Commission on Stratigraphic Nomenclature NASC (2005) North American Stratigraphic Code.
630 Bull Am Assoc Petrol Geol 89:1547-1591. doi:10.1306/07050504129

631 Ori GG (1993) Continental depositional systems of the Quaternary of the Po plain (Northern Italy). Sediment Geol
632 83:1-14. doi:10.1016/S0037-0738(10)80001-6

633 Pellegrini L, Boni P, Carton A (2003) Hydrographic evolution in relation to neotectonics aided by data processing
634 and assessment: some examples from the Northern Apennines (Italy). Quat Inter 101-102:211-217.
635 doi:10.1016/S1040-6182(02)00103-9

636 Pieri M, Groppi G (1981) Subsurface geological structure of the Po plain, Italy. Progetto Finalizzato Geodinamica,
637 Pubbl. 411. 13 pp., CNR, Roma

638 Pirson (1958) Elements of Oil Reservoir Engineering. 2nd edition. McGraw Hill, 608 pp., New York.

639 Reynolds JM (2011) An Introduction to Applied and Environmental Geophysics. 696 pp., Wiley-Blackwell,
640 Chichester,UK

641 Rossi M, Minervini M, Ghielmi M, Rogledi S (2015) Messinian and Pliocene erosional surfaces in the Po Plain-
642 Adriatic Basin: Insights from allostratigraphy and sequence stratigraphy in assessing play concepts related to

643 accommodation and gateway turnarounds in tectonically active margins. Mar Petrol Geol 66:192-216. doi:
644 10.1016/j.marpetgeo.2014.12.012

645 Rubin Y, Hubbard SS (2005) Hydrogeophysics. Springer, 527 pp., Dordrecht, The Netherlands

646 Scardia G, Muttoni G, Sciunnach D (2006) Subsurface magnetostratigraphy of Pleistocene sediments from the Po
647 Plain (Italy): Constraints on rates of sedimentation and rock uplift. Geol Soc Am Bull 118:1299–1312.
648 doi:10.1130/B25869.1.

649 Scardia G, De Franco R, Muttoni G, Rogledi S, Caielli G, Carcano C, Sciunnach D, Piccin A (2012) Stratigraphic
650 evidence of a Middle Pleistocene climate-driven flexural uplift in the Alps. Tectonics 31:TC6004.
651 doi:10.1029/2012TC003108

652 Schön JH (2004) Physical properties of rocks: Fundamentals and Principles of Petrophysics, 583 pp., Elsevier,
653 Amsterdam

654 Sistema Informativo Ambientale SIA, Città metropolitana di Milano,
655 http://ambiente.provincia.milano.it/sia/ot/acqsot/contenutisot.asp?rif1=H2Osot&rif2=H2Osot&idrf=0 accessed April
656 2017

657 Slater L (2007) Near Surface Electrical Characterization of Hydraulic Conductivity: From Petrophysical Properties
658 to Aquifer Geometries - a review. Surv Geophys 28:169-197. doi:10.1007/s10712-007-9022-y

659 Telford WM, Geldart LP, Sheriff RE (1990) Applied geophysics, 2nd edition. 770 pp., Cambridge University Press,
660 Cambridge.

661 Toscani G, Bonini L, Irfan AM, Di Bucci D, Di Giulio A, Seno S, Galuppo C (2014) Opposite verging chains
662 sharing the same foreland: Kinematics and interactions through analogue models (Central Po Plain, Italy).
663 Tectonophysics 633:268-282. doi: 10.1016/j.tecto.2014.07.019

664 Turrini C, Lacombe O, Roure, F, (2014) Present-day 3D structural model of the Po Valley basin, Northern Italy.
665 Mar Petrol Geol 56, 266–289. doi:10.1016/j.marpetgeo.2014.02.006.

Zuffetti C, Bersezio R, Contini D, Petrizzo MR (2018) Geology of the San Colombano hill, a Quaternary isolated tectonic relief in the Po Plain of Lombardy (Northern Italy), Journal of Maps, 14:2, 199-211, DOI: 10.1080/17445647.2018.1443166

8. FIGURE CAPTIONS

Fig. 1. Simplified geomorphological map and main subsurface tectonic features of the Quaternary Po foredeep basin in Lombardy (after Bigi et al. 1990; Castiglioni and Pellegrini 2001; Fantoni et al. 2004). The map shows the location of VES surveys and the trace of the resistivity cross-section (black line) in the interfluve between the Adda and Lambro Holocene valleys. Location of the map in Northern Italy is indicated in the top left insert.

Fig. 2. Box A) Apparent resistivity curves of VES along the resistivity cross-section (location in Fig. 1). Box B) Horizontal variation of apparent electrical resistivity measured along the cross-section for a Schlumberger array and half-spacings between the current electrodes equal to 10 m (red line), 60 m (green line), 300 m (blue line).

Fig. 3: Example of multiple electro-layer interpretation at VES T7 (location in Fig. 1). On the left: the resistivity-versus-depth profile is shown with the hierarchic interfaces traced along the cross-section shown later in Fig. 5 and the litho-textural logs for comparison. On the right: multilayer interpretation obtained by complete curve matching (from 3- to 7- layers models, reducing RMS % error), showing the comparison of subsurface structure in terms of pattern of the interfaces and the corresponding depth variability.

Fig. 4: Example of the hierarchical procedure to trace the electrostratigraphic interfaces starting from 1-D models obtained by curve-matching of single VES (zoom in from the northern and shallower sector of the regional resistivity cross-section, zoom box shown in Fig. 5). The modelled 1-D resistivity for individual electrolayers is displayed at each VES location; the polarity across individual electrostratigraphic interfaces (relative resistive over conductive or vice-versa) is also represented with double coloured lines (red and blue, respectively, along the resistive and conductive faces). Note that high-, intermediate- and low-order electrical interfaces bound adjacent and overlapping units of comparable rank preserving the reciprocal polarity wherever it is traceable.

Fig. 5: Electrostratigraphic cross-section across the Po plain (location in Fig. 1) showing the architecture of electrostratigraphy (see legend for hierarchy of units). Litho-textural logs are orthogonally projected from a maximum

692 distance of 300 m (litho-textural classes: G: gravel; S: sand, L: silt: C: clay; f: fine; m: medium, c: coarse). Vertical
693 exaggeration: 100×.

694 Fig. 6: Box A) Vertical resistivity trends of 1st order groups of EsUs. Box B) horizontal resistivity trends within
695 individual 2nd order EsUs. Resistivity trends are represented with coloured triangular sticks with apex in the direction
696 of decreasing resistivity. Colours help to differentiate the 2nd order more conductive EsUs (same as Fig. 5). The S1-S4
697 1st order boundaries between 1st order Groups are coloured as in Fig. 5.
698

699 ## 9. TABLE CAPTIONS

700 Tab. 1: Electrostratigraphic sequence of the central Po Plain in Lombardy. Refer to Fig. 4 and 5 to visualize
701 individual EsUs, EsU Groups and the relative Bounding Surfaces (1st order: S1 to S4) and to Fig. 6 for Vertical vs.
702 Horizontal Resistivity trends. Two orders of the hierarchic assemblage are shown: Groups of EsUs (1st order) and
703 EsUs (2nd order).

704

705 Table 1

GROUP OF ESUS (1ST ORDER)	RESISTIVITY RANGE IN Ωm OF THE 2ND ORDER ESUS	GEOMETRY & STACKING PATTERN	INTERPRETED HYDROSTRATIGRAPHY
1	25 to 67, red in Fig.4	Gently dipping, alternating R/C wedges with decreasing vs. increasing upward resistivity trends	Phreatic to semi-confined freshwater aquifers/aquitards
	71 to 192 pink in Fig.4		
	72 to 1109, white in Fig.4		
2	33 to 93 dark yellow in Fig.4	Curved resistive wedge with upward decreasing resistivity trend	Semi-confined freshwater aquifers
	99 to 173 light yellow in Fig.4		
3	25 to 69 dark green in Fig.4	Curved resistive body with upward decreasing resistivity trend and intervening resistive lenses with homogenous resistivity values	Confined freshwater aquifers.
	81 to 214 light green in Fig.4		
4	14 to 26 dark blue in Fig.4	resistive lenses within widespread conductive	Basal confining layer with fresh- brackish water isolated aquifers.
	21 to 48 cyan in Fig.4		
	65 to 217 light blue in Fig.4		
5	< 9 grey in Fig.4	Curved, up-doming conductive layer	Saltwater basal aquitard

706

707

708 Figure 1

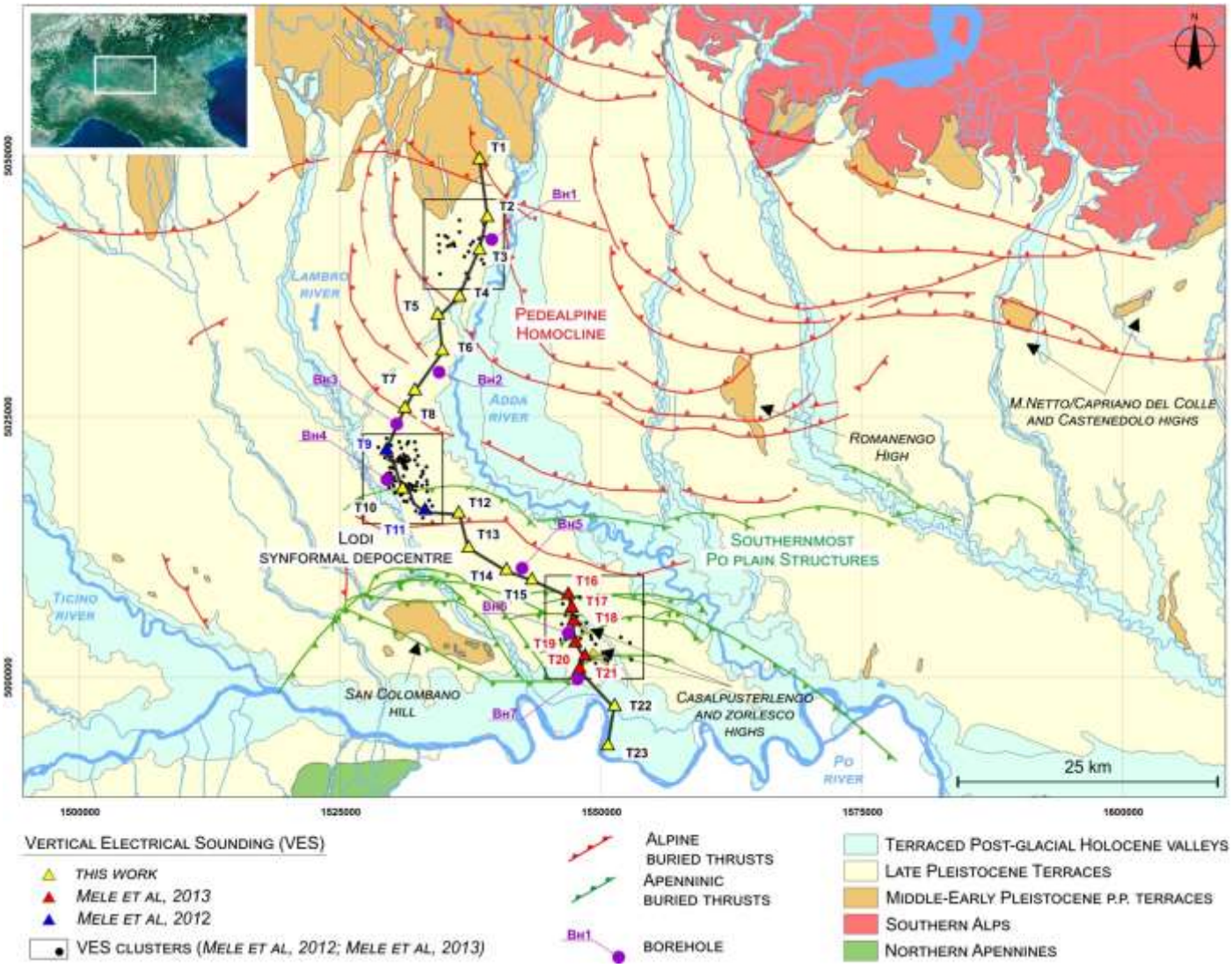

709

710

Figure 2

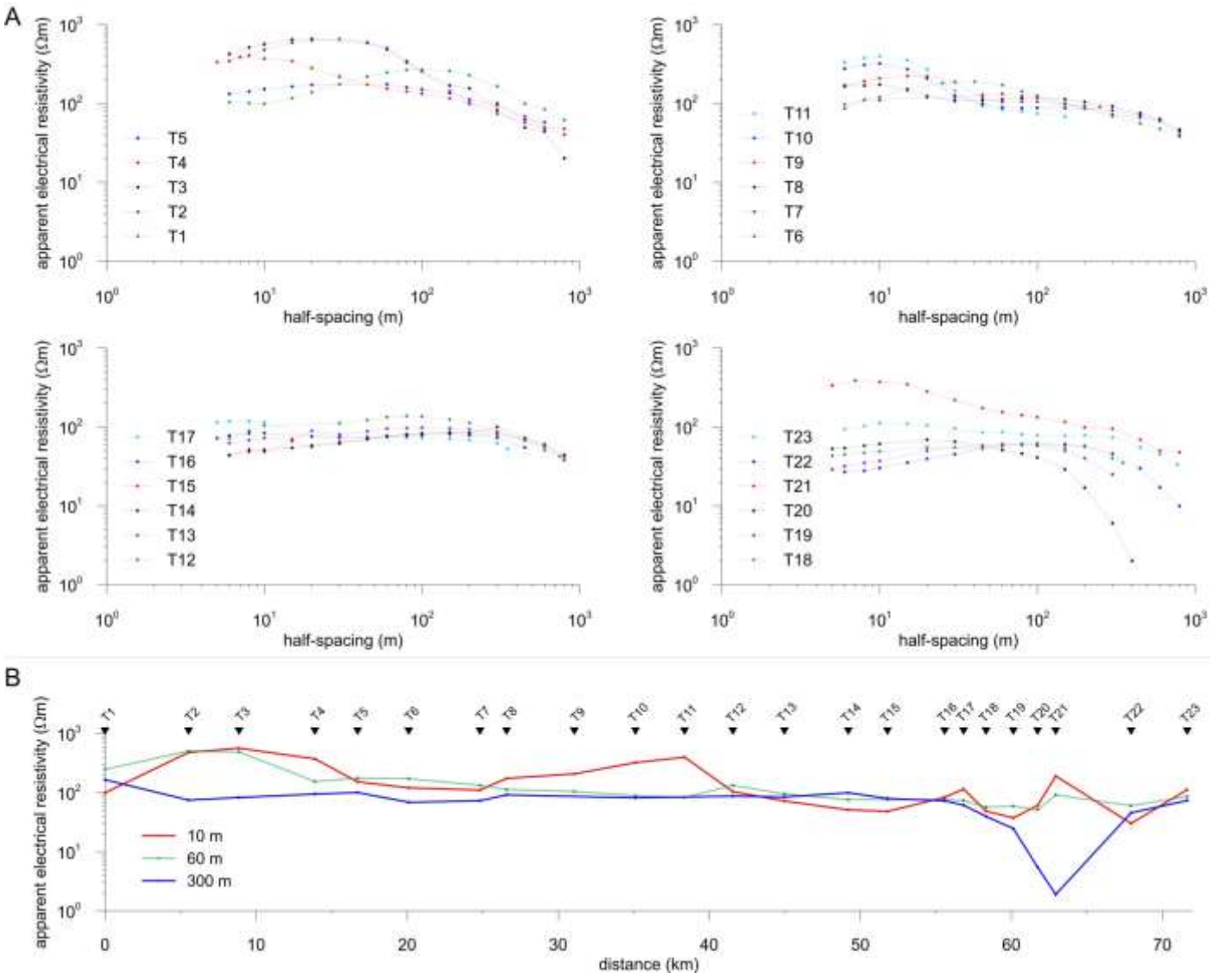
A
apparent electrical resistivity (Ωm)
half-spacing (m)
T5
T4
T3
T2
T1
T11
T10
T9
T8
T7
T6
T17
T16
T15
T14
T13
T12
T23
T22
T21
T20
T19
T18
B
distance (km)
10 m
60 m
300 m

714 Figure 3

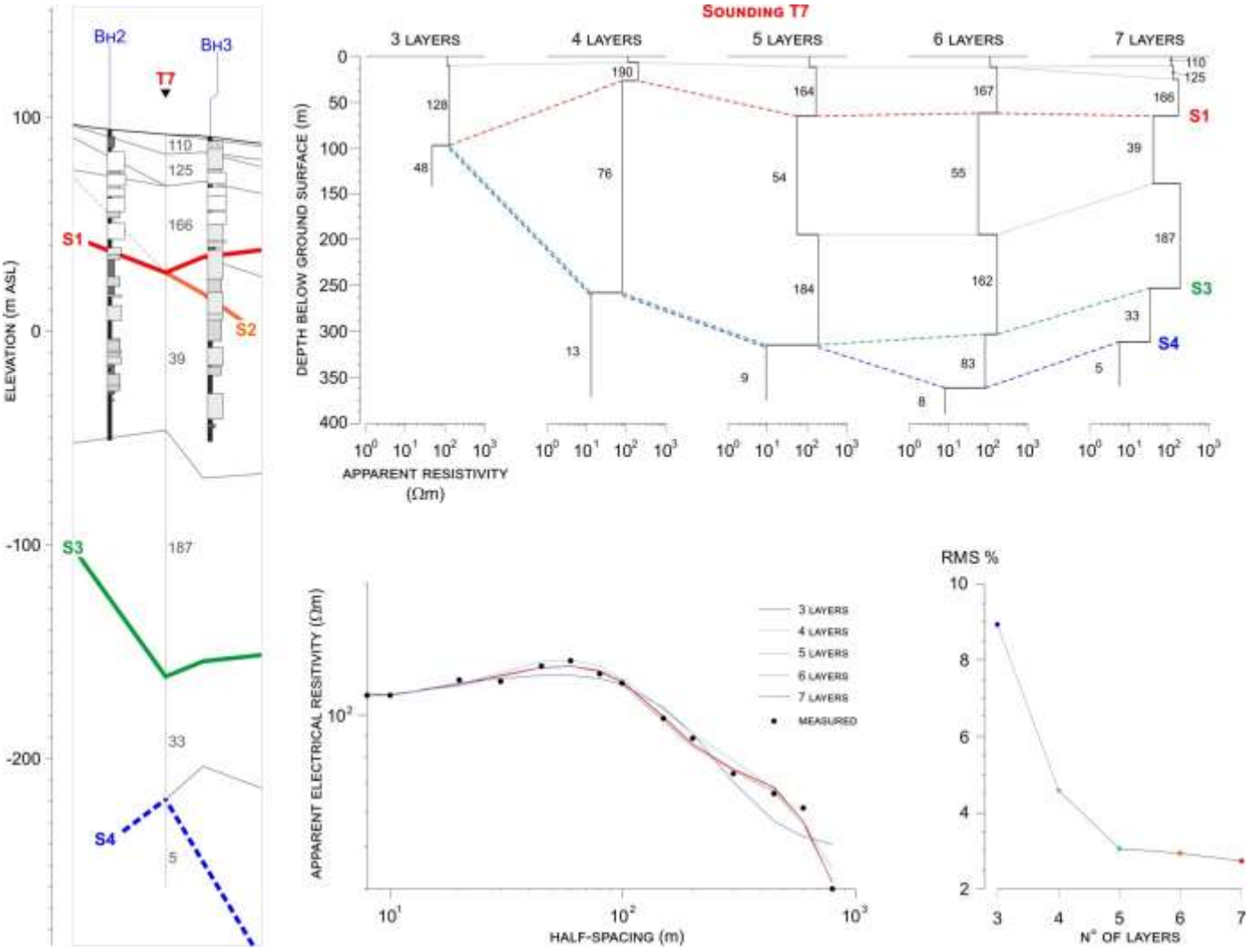

715

716

Figure 4

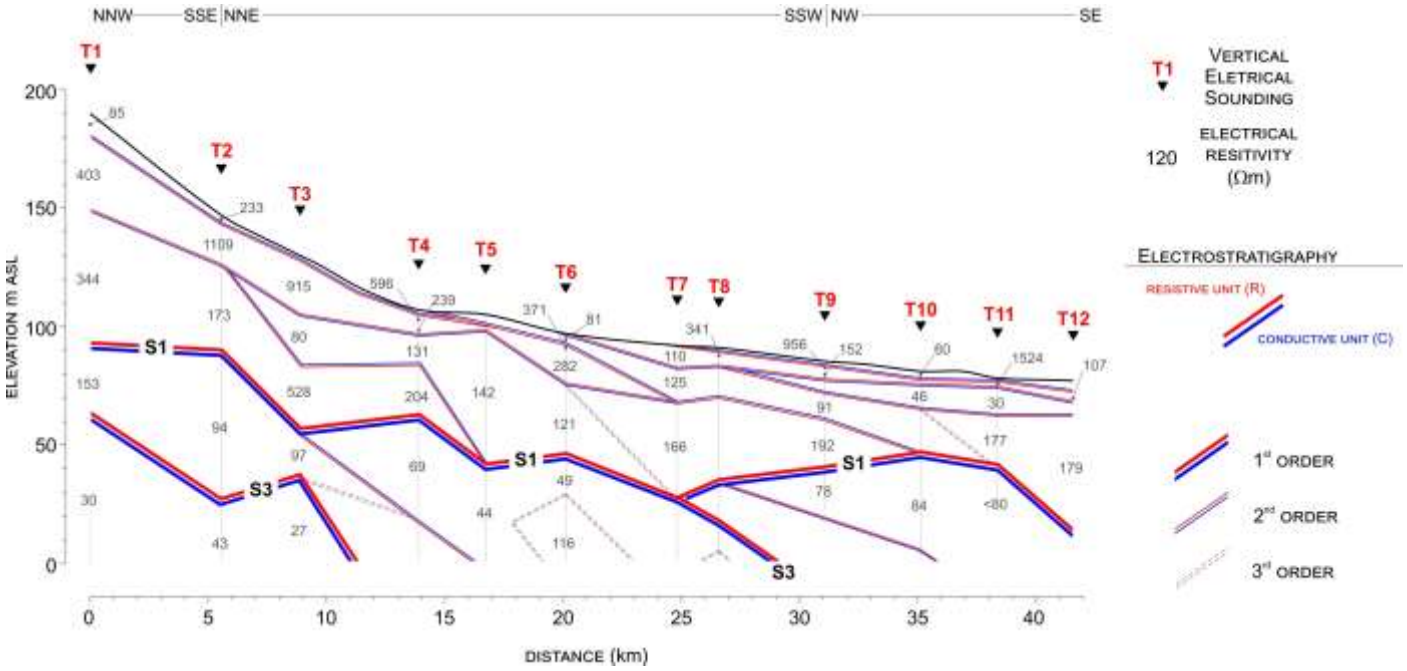
NNW
SSE
NNE
SSW
NW
SE
T1
T2
T3
T4
T5
T6
T7
T8
T9
T10
T11
T12
S1
S3
ELEVATION m ASL
DISTANCE (km)
VERTICAL ELETRICAL SOUNDING
ELECTRICAL RESITIVITY (Ωm)
120
ELECTROSTRATIGRAPHY
RESISTIVE UNIT (R)
CONDUCTIVE UNIT (C)
1st ORDER
2nd ORDER
3rd ORDER

720 Figure 5

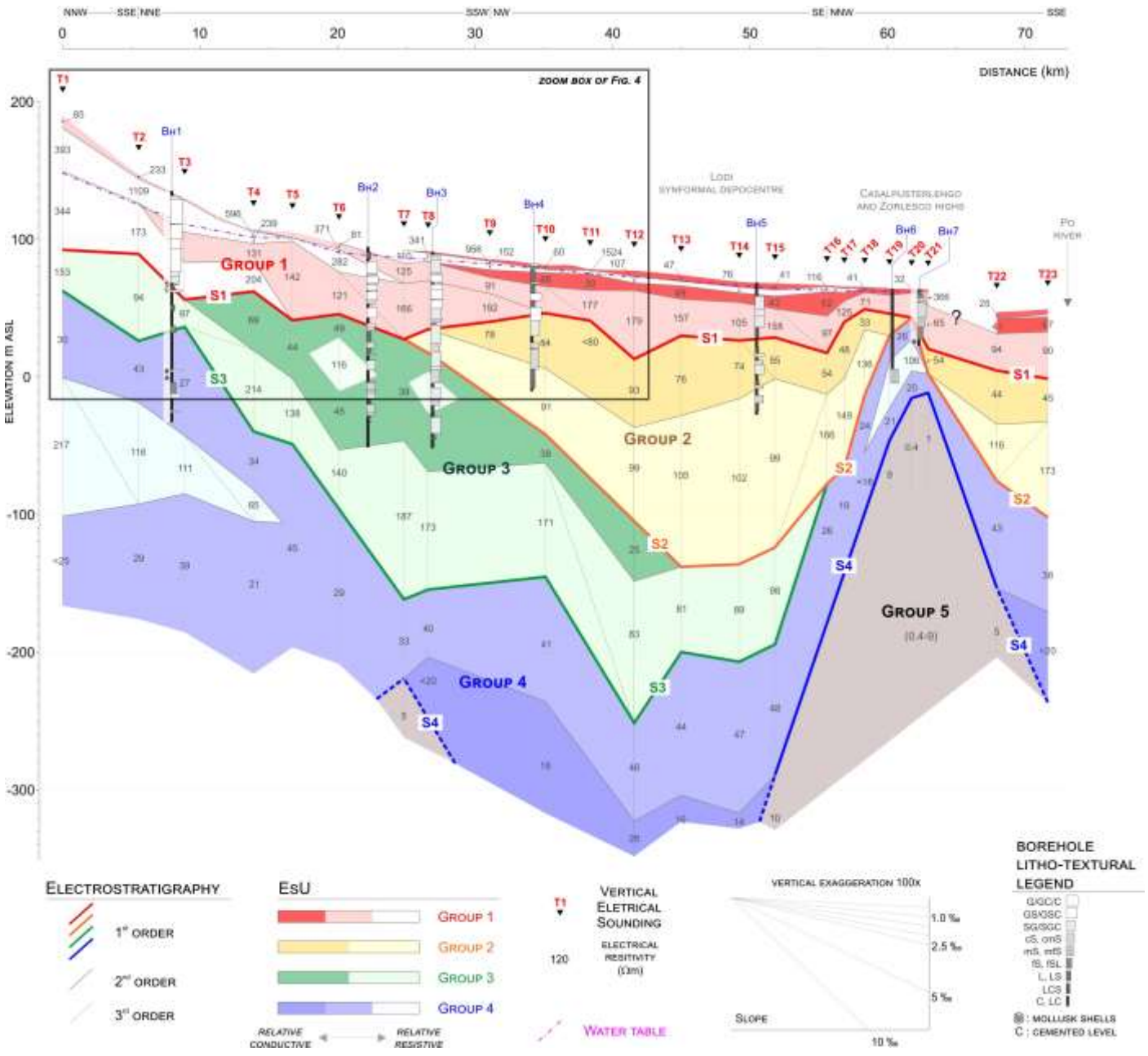

721

722

723 Figure 6

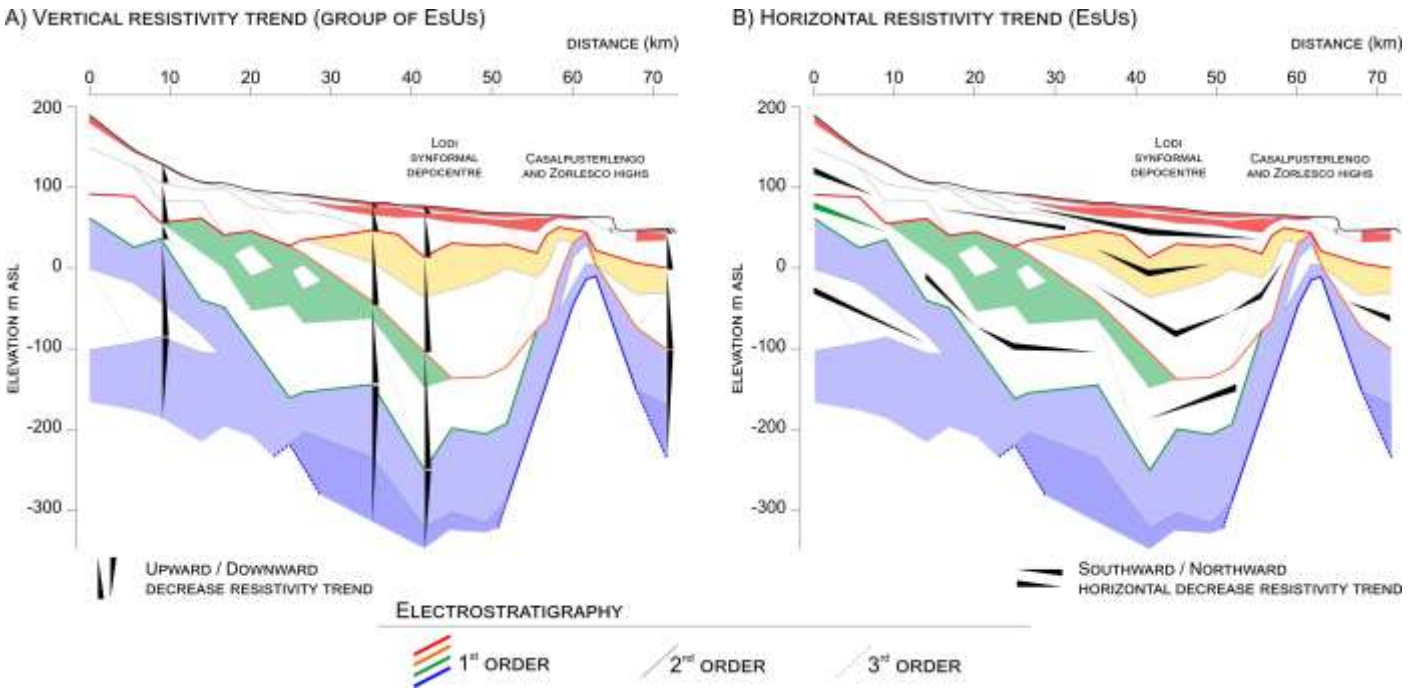

724

725